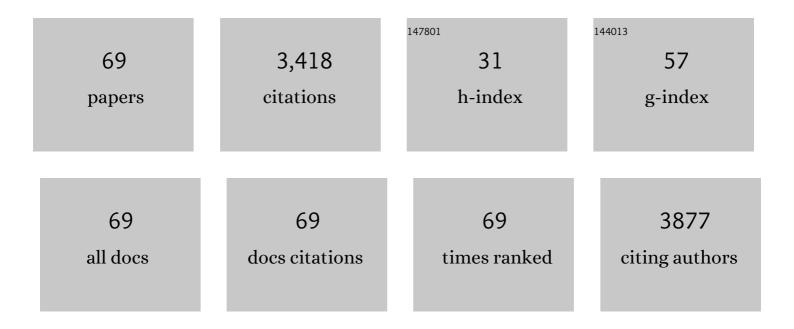
Xh Zheng

List of Publications by Year in descending order

Source: https://exaly.com/author-pdf/1464935/publications.pdf Version: 2024-02-01



#	Article	IF	CITATIONS
1	Defectâ€Rich Heterogeneous MoS ₂ /NiS ₂ Nanosheets Electrocatalysts for Efficient Overall Water Splitting. Advanced Science, 2019, 6, 1900246.	11.2	468
2	Hierarchical NiCo-LDH/NiCoP@NiMn-LDH hybrid electrodes on carbon cloth for excellent supercapacitors. Journal of Materials Chemistry A, 2018, 6, 15040-15046.	10.3	233
3	Activating and optimizing the activity of NiCoP nanosheets for electrocatalytic alkaline water splitting through the V doping effect enhanced by P vacancies. Journal of Materials Chemistry A, 2019, 7, 24486-24492.	10.3	227
4	Core-branched CoSe ₂ /Ni _{0.85} Se nanotube arrays on Ni foam with remarkable electrochemical performance for hybrid supercapacitors. Journal of Materials Chemistry A, 2018, 6, 19151-19158.	10.3	171
5	Atomic scale insights into structure instability and decomposition pathway of methylammonium lead iodide perovskite. Nature Communications, 2018, 9, 4807.	12.8	161
6	Nanoarchitectured Design of Vertical‣tanding Arrays for Supercapacitors: Progress, Challenges, and Perspectives. Advanced Functional Materials, 2021, 31, 2006030.	14.9	150
7	Bifunctional Electrocatalysts Based on Mo-Doped NiCoP Nanosheet Arrays for Overall Water Splitting. Nano-Micro Letters, 2019, 11, 55.	27.0	125
8	In Situ Synthesis of Vertical Standing Nanosized NiO Encapsulated in Graphene as Electrodes for Highâ€Performance Supercapacitors. Advanced Science, 2018, 5, 1700687.	11.2	117
9	Atomic‣evel Platinum Filling into Niâ€Vacancies of Dualâ€Deficient NiO for Boosting Electrocatalytic Hydrogen Evolution. Advanced Energy Materials, 2022, 12, .	19.5	110
10	<i>In situ</i> encapsulated Fe ₃ O ₄ nanosheet arrays with graphene layers as an anode for high-performance asymmetric supercapacitors. Journal of Materials Chemistry A, 2017, 5, 24594-24601.	10.3	105
11	Designing oxygen bonding between reduced graphene oxide and multishelled Mn ₃ O ₄ hollow spheres for enhanced performance of supercapacitors. Journal of Materials Chemistry A, 2019, 7, 6686-6694.	10.3	103
12	Corrosion behavior of stainless steel-tungsten carbide joints brazed with AgCuX (XÂ=ÂIn, Ti) alloys. Corrosion Science, 2022, 200, 110231.	6.6	80
13	P-Doped NiCo ₂ S ₄ nanotubes as battery-type electrodes for high-performance asymmetric supercapacitors. Dalton Transactions, 2018, 47, 8771-8778.	3.3	75
14	Oxygen-vacancy-rich nickel-cobalt layered double hydroxide electrode for high-performance supercapacitors. Journal of Colloid and Interface Science, 2019, 554, 59-65.	9.4	70
15	Designing and constructing core-shell NiCo2S4@Ni3S2 on Ni foam by facile one-step strategy as advanced battery-type electrodes for supercapattery. Journal of Colloid and Interface Science, 2019, 536, 456-462.	9.4	70
16	Mesostructured Carbon Nanotube-on-MnO ₂ Nanosheet Composite for High-Performance Supercapacitors. ACS Applied Materials & Interfaces, 2018, 10, 38963-38969.	8.0	65
17	Hierarchical CuCo ₂ O ₄ @NiMoO ₄ core–shell hybrid arrays as a battery-like electrode for supercapacitors. Inorganic Chemistry Frontiers, 2017, 4, 1575-1581.	6.0	55
18	Thermal stability and high-temperature shape memory effect of Ti–Ta–Zr alloy. Scripta Materialia, 2013, 68, 1008-1011.	5.2	50

Xh Zheng

#	Article	IF	CITATIONS
19	Free-standing porous Ni2P-Ni5P4 heterostructured arrays for efficient electrocatalytic water splitting. Journal of Colloid and Interface Science, 2019, 552, 332-336.	9.4	49
20	W doping dominated NiO/NiS2 interfaced nanosheets for highly efficient overall water splitting. Journal of Colloid and Interface Science, 2020, 562, 363-369.	9.4	47
21	Fe doped Ni ₅ P ₄ nanosheet arrays with rich P vacancies <i>via</i> phase transformation for efficient overall water splitting. Nanoscale, 2020, 12, 6204-6210.	5.6	47
22	Engineering Se vacancies to promote the intrinsic activities of P doped NiSe2 nanosheets for overall water splitting. Journal of Colloid and Interface Science, 2020, 571, 260-266.	9.4	47
23	Modifying the electrochemical performance of vertically-oriented few-layered graphene through rotary plasma processing. Journal of Materials Chemistry A, 2018, 6, 908-917.	10.3	46
24	Welding and Joining of Titanium Aluminides. Materials, 2014, 7, 4930-4962.	2.9	45
25	Hierarchical Fe2O3 and NiO nanotube arrays as advanced anode and cathode electrodes for high-performance asymmetric supercapacitors. Journal of Alloys and Compounds, 2019, 794, 255-260.	5.5	45
26	Rich P vacancies modulate Ni2P/Cu3P interfaced nanosheets for electrocatalytic alkaline water splitting. Journal of Colloid and Interface Science, 2020, 564, 37-42.	9.4	43
27	General Decomposition Pathway of Organic–Inorganic Hybrid Perovskites through an Intermediate Superstructure and its Suppression Mechanism. Advanced Materials, 2020, 32, e2001107.	21.0	42
28	Exploring CoP core–shell nanosheets by Fe and Zn dual cation doping as efficient electrocatalysts for overall water splitting. Catalysis Science and Technology, 2020, 10, 1395-1400.	4.1	40
29	Rational construction of core–shell Ni3S2@Ni(OH)2 nanostructures as battery-like electrodes for supercapacitors. Inorganic Chemistry Frontiers, 2018, 5, 1985-1991.	6.0	37
30	Nickel-doped MoSe2 nanosheets with Ni–Se bond for alkaline electrocatalytic hydrogen evolution. International Journal of Hydrogen Energy, 2020, 45, 10724-10728.	7.1	37
31	Atomic-scale imaging of CH3NH3PbI3 structure and its decomposition pathway. Nature Communications, 2021, 12, 5516.	12.8	36
32	In situ synthesis of core-shell vanadium nitride@N-doped carbon microsheet sponges as high-performance anode materials for solid-state supercapacitors. Journal of Colloid and Interface Science, 2020, 560, 122-129.	9.4	34
33	A fast micro–nano liquid layer induced construction of scaled-up oxyhydroxide based electrocatalysts for alkaline water splitting. Journal of Materials Chemistry A, 2021, 9, 26777-26787.	10.3	27
34	Mn and S dual-doping of MOF-derived Co3O4 electrode array increases the efficiency of electrocatalytic generation of oxygen. Journal of Colloid and Interface Science, 2019, 557, 28-33.	9.4	26
35	All-in-One Sulfur Host: Smart Controls of Architecture and Composition for Accelerated Liquid–Solid Redox Conversion in Lithium–Sulfur Batteries. ACS Applied Materials & Interfaces, 2021, 13, 39424-39434.	8.0	22
36	Synthesis of graphene on a Ni film by radio-frequency plasma-enhanced chemical vapor deposition. Science Bulletin, 2012, 57, 3040-3044.	1.7	21

Xh Zheng

#	Article	IF	CITATIONS
37	Effect of Ni substitution for Ga on the polycrystalline Ni–Mn–Ga–Gd high-temperature shape memory alloys. Journal of Alloys and Compounds, 2013, 557, 60-66.	5.5	21
38	Sea urchin-like CuCo ₂ S ₄ microspheres with a controllable interior structure as advanced electrode materials for high-performance supercapacitors. Inorganic Chemistry Frontiers, 2020, 7, 603-609.	6.0	20
39	Self-Assembly Lightweight Honeycomb-Like Prussian Blue Analogue on Cu Foam for Lithium Metal Anode. ACS Applied Materials & Interfaces, 2021, 13, 23803-23810.	8.0	19
40	Lattice Mismatch in Ni ₃ Se ₄ –MoSe ₂ Nanoheterostructures with an Abundant Interface for Catalytic Hydrogen Evolution. ACS Applied Nano Materials, 2021, 4, 3493-3499.	5.0	18
41	Constructing MoS ₂ /CoMo ₂ S ₄ /Co ₃ S ₄ nanostructures supported by graphene layers as the anode for lithium-ion batteries. Dalton Transactions, 2020, 49, 1167-1172.	3.3	17
42	In situ formation of TiB whiskers to reinforce SiO2-BN/Ti6Al4V brazed joints. Ceramics International, 2019, 45, 8054-8057.	4.8	16
43	Tailoring the microstructure, martensitic transformation and strain recovery characteristics of Ti-Ta shape memory alloys by changing Hf content. Journal of Materials Science and Technology, 2021, 83, 123-130.	10.7	16
44	Surface activation towards manganese dioxide nanosheet arrays via plasma engineering as cathode and anode for efficient water splitting. Journal of Colloid and Interface Science, 2021, 586, 95-102.	9.4	15
45	Characterization of free-standing nanocrystalline Ni 55.2 Mn 24.7 Ga 19.9 Gd 0.2 high temperature shape memory thin film. Journal of Alloys and Compounds, 2016, 661, 43-48.	5.5	11
46	Antimony nanocrystals self-encapsulated within bio-oil derived carbon for ultra-stable sodium storage. Journal of Colloid and Interface Science, 2021, 582, 459-466.	9.4	11
47	Plasma-induced surface reorganization of porous Co3O4-CoO heterostructured nanosheets for electrocatalytic water oxidation. Journal of Colloid and Interface Science, 2020, 565, 400-404.	9.4	10
48	Bioinspired Metal-Intermetallic Laminated Composites for the Fabrication of Superhydrophobic Surfaces with Responsive Wettability. ACS Applied Materials & Interfaces, 2021, 13, 5834-5843.	8.0	10
49	Stable lithium metal anode achieved by shortening diffusion path on solid electrolyte interface derived from Cu2O lithiophilic layer. Chemical Engineering Journal, 2022, 433, 133689.	12.7	10
50	Thermal stability of Ni54Mn25Ga20.9Gd0.1 high-temperature shape memory alloy with large reversible strain. Materials Letters, 2014, 123, 250-253.	2.6	9
51	Direct Observation of Li Migration into V ₅ S ₈ : Order to Antisite Disorder Intercalation Followed by the Topotactic-Based Conversion Reaction. ACS Applied Materials & Interfaces, 2020, 12, 36320-36328.	8.0	9
52	Making Superhydrophobic Surfaces with Microstripe Array Structure by Diffusion Bonding and Their Applications in Magnetic Control Microdroplet Release Systems. Advanced Materials Interfaces, 2017, 4, 1700918.	3.7	8
53	The effect of annealing treatment on microstructure and shape memory behavior of Ti-Ta-Zr thin films. Vacuum, 2018, 153, 1-5.	3.5	8
54	Atomic-scale structural and chemical evolution of Li3V2(PO4)3 cathode cycled at high voltage window. Nano Research, 2019, 12, 1675-1681.	10.4	8

XH ZHENG

#	Article	IF	CITATIONS
55	Constructing NiS–VS heterostructured nanosheets for efficient overall water splitting. Inorganic Chemistry Frontiers, 2020, 7, 4924-4929.	6.0	7
56	Rationally designed C/Co ₉ S ₈ @SnS ₂ nanocomposite as a highly efficient anode for lithium-ion batteries. Nanotechnology, 2020, 31, 395401.	2.6	7
57	Periodic Corrosion Turns Bulk Ni into Zr-Incorporated Polycrystalline Ni(OH) ₂ Nanoarrays for Overall Water Decomposition. ACS Applied Energy Materials, 2022, 5, 5711-5718.	5.1	7
58	Understanding the Effect of Surface Machining on the YSZ/Ti6Al4V Joint via Image Based Modelling. Scientific Reports, 2019, 9, 12027.	3.3	6
59	Thermal stability and high-temperature shape memory effect of Ni 55.2 Mn 24.7 Ga 19.9 Gd 0.2 thin film. Vacuum, 2018, 147, 78-81.	3.5	5
60	Cu-Based Multicomponent Metallic Compound Materials as Electrocatalyst for Water Splitting. Frontiers in Chemistry, 0, 10, .	3.6	5
61	Highâ€Performance Supercapacitors: In Situ Synthesis of Vertical Standing Nanosized NiO Encapsulated in Graphene as Electrodes for Highâ€Performance Supercapacitors (Adv. Sci. 3/2018). Advanced Science, 2018, 5, 1870019.	11.2	4
62	Facile Synthesis of FeOOHâ^'Ni ₃ S ₂ Nanosheet Arrays on Nickel Foam via Chemical Immersion toward Electrocatalytic Water Splitting. ChemistrySelect, 2022, 7, .	1.5	4
63	Joining 3YSZ Electrolyte to AISI 441 Interconnect Using the Ag Particle Interlayer: Enhanced Mechanical and Aging Properties. Crystals, 2021, 11, 1573.	2.2	3
64	The effects of indium addition on mechanical properties and shape memory behavior of Ti-Ta-Zr high temperature alloys. Materials Chemistry and Physics, 2020, 249, 123189.	4.0	2
65	Joining Alumina and Sapphire by Growing Aluminium Borate Whiskers In-Situ, and the Whiskers' Orientation Relationship with the Sapphire Substrate. Materials, 2020, 13, 175.	2.9	2
66	Microstructure and mechanical properties of Al ₂ O ₃ ceramic joints achieved by Ag‣iO ₂ braze in air. International Journal of Applied Ceramic Technology, 2022, 19, 508-513.	2.1	2
67	Damping Capacity of Ni–Mn–Ga–Gd High-Temperature Shape Memory Thin Film. Shape Memory and Superelasticity, 2018, 4, 369-376.	2.2	1
68	Effect of Ni concentration on solderability, microstructure and hardness of SAC0705-xNi solder joints on Cu and graphene-coated Cu substrates. Modern Physics Letters B, 2019, 33, 1850425.	1.9	1
69	Superhydrophobicity: Making Superhydrophobic Surfaces with Microstripe Array Structure by Diffusion Bonding and Their Applications in Magnetic Control Microdroplet Release Systems (Adv.) Ti ETOq1 1	0.784314	gB&/Overloo